

Impact of Pressure and Apical Oxygen Vacancies on Superconductivity in $\text{La}_3\text{Ni}_2\text{O}_7$

Chen Lu,^{1,*} Ming Zhang,^{2,*} Zhiming Pan,^{3,*} Congjun Wu,^{4,5,6,7} and Fan Yang^{8,†}

¹*School of Physics, Hangzhou Normal University, Hangzhou 311121, China*

²*Zhejiang Key Laboratory of Quantum State Control and Optical Field Manipulation,*

Department of Physics, Zhejiang Sci-Tech University, 310018 Hangzhou, China

³*Department of Physics, Xiamen University, Xiamen 361005, Fujian, China*

⁴*New Cornerstone Science Laboratory, Department of Physics,*

School of Science, Westlake University, Hangzhou 310024, Zhejiang, China

⁵*Institute for Theoretical Sciences, Westlake University, Hangzhou 310024, Zhejiang, China*

⁶*Key Laboratory for Quantum Materials of Zhejiang Province,*

School of Science, Westlake University, Hangzhou 310024, Zhejiang, China

⁷*Institute of Natural Sciences, Westlake Institute for Advanced Study, Hangzhou 310024, Zhejiang, China*

⁸*School of Physics, Beijing Institute of Technology, Beijing 100081, China*

The bilayer nickelate $\text{La}_3\text{Ni}_2\text{O}_7$ under pressure has recently emerged as a promising system for high- T_c superconductivity (SC). In this work, we investigate the fate of the SC properties in $\text{La}_3\text{Ni}_2\text{O}_7$ under pressure, focusing on the effects of structural deformation and apical oxygen vacancies. Employing a low-energy effective t - J_{\parallel} - J_{\perp} model for the $3d_{x^2-y^2}$ orbitals within the slave-boson mean-field approach, we demonstrate that the SC pairing strength is significantly enhanced in the high-pressure tetragonal $I4/mmm$ phase compared to the ambient pressure orthorhombic $Amam$ phase. Furthermore, by simulating random configurations of apical oxygen vacancies, we show that oxygen vacancies suppress both pairing strength and superfluid density. These results underscore the critical role of pressure and oxygen stoichiometry in tuning the SC of $\text{La}_3\text{Ni}_2\text{O}_7$, providing key insights into optimizing its high- T_c behavior.

Introduction

Ruddlesden-Popper (RP) phase nickelates series $\text{La}_{n+1}\text{Ni}_n\text{O}_{3n+1}$ have been a subject of sustained and intense research due to their potential for realizing high- T_c superconductivity (SC) [1–18]. In a recent pivotal development, superconducting phenomena exhibiting a critical temperature T_c of approximately 80K was discovered in $\text{La}_3\text{Ni}_2\text{O}_7$ ($n = 2$) under a pressure exceeding 14 GPa [19–24], attracting great interests [24–84]. Furthermore, realization of SC with a critical $T_c \approx 40\text{K}$ in $\text{La}_3\text{Ni}_2\text{O}_7$ thin films under ambient pressure [85, 86], represents a crucial step forward towards practical applications and experimental investigations [87–90]. Additionally, experimental evidence of SC with a $T_c \approx 20\text{K}$ in another RP-phase material, $\text{La}_4\text{Ni}_3\text{O}_{10}$ ($n = 3$) [91–93], has also attracted significant attention [33, 94–118]. A recent discovery of SC was found in $\text{La}_5\text{Ni}_3\text{O}_{11}$ under pressure with $T_c \approx 60\text{K}$ [119].

The phase diagram of $\text{La}_3\text{Ni}_2\text{O}_7$ has been explicitly explored across a wide range of temperatures and pressures [19, 120], revealing a complex and rich phenomenology. In particular, the complex nature of the phase diagram and the potential for unconventional SC have attracted a subsequent surge of theoretical investigations aimed at revealing the underlying SC mechanism [47–73, 75–84]. Despite these intensive theoretical efforts, the precise nature of the superconducting pairing mechanism in $\text{La}_3\text{Ni}_2\text{O}_7$ remains an open question and a subject of ongoing debate. Two key factors, pressure and oxygen stoichiometry, play important role and complicate the problem.

Experimental studies have definitively demonstrated

that the emergence of SC in $\text{La}_3\text{Ni}_2\text{O}_7$ is strongly and sensitively influenced by the application of external pressure [19–24, 27–29, 45]. At ambient pressure, the material exhibits a metallic state characterized by weakly insulating behavior at low temperatures. Under enough pressure, $\text{La}_3\text{Ni}_2\text{O}_7$ undergoes a structural phase transition from the orthorhombic $Amam$ phase at ambient pressure (AP) to the tetragonal $I4/mmm$ phase under high pressure (HP) around 14 GPa. This transition is accompanied by the inter-bilayer Ni-O-Ni bond angle evolving from 168° to 180° [19], leading to a significantly enhanced inter-bilayer coupling. Subsequently, SC rapidly emerges at higher pressures, with optimal T_c peaking at 83 K near 18 GPa. Further increasing the pressure leads to a gradual decline in T_c , resulting in a distinctive right-triangle-shaped superconducting region in the phase diagram [120].

The realization of SC is also highly sensitive to oxygen stoichiometry [29, 36, 42, 43, 46, 85, 89, 120], emphasizing that sufficient oxygen content is crucial for stabilizing robust SC [49, 84, 121]. Oxygen vacancies significantly alter the electronic structure and orbital interactions critical to SC. Experimental observations, including scanning transmission electron microscopy (STEM) and X-ray diffraction (XRD) [42, 120], have provided direct visualization of oxygen vacancies, particularly attributed to apical oxygen sites. Transport measurements have revealed that oxygen vacancies can reduce the superconducting volume fraction and, in some samples, induce a filamentary SC state [85]. Additionally, ozone annealing has been employed to manipulate oxygen stoichiometry, further demonstrating the importance of oxygen control

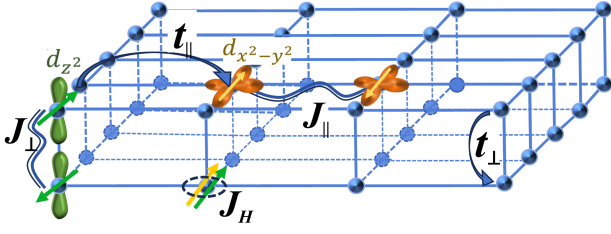


FIG. 1. (color online) Schematic illustration of the two-orbital bilayer t - J - J_H model. The charge carriers primarily reside in the $3d_{x^2-y^2}$ orbitals, as indicated with wavy lines on the lattice, while the $3d_{z^2}$ orbitals are depicted as localized spins due to their single occupancy. These localized spins interact via interlayer spin exchange J_{\perp} , reflecting the strong correlations present in the system. The onsite E_g orbitals tend to form a spin-triplet configuration driven by Hund's rule coupling J_H .

in optimizing SC [89].

In this paper, we employ strong correlated analysis to investigate the effects of pressure and random apical oxygen vacancies on the superconducting properties of $\text{La}_3\text{Ni}_2\text{O}_7$. We adopt a minimal low-energy t - J_{\parallel} - J_{\perp} model for the Ni $3d_{x^2-y^2}$ orbital [54] for the understanding of the SC. Our numerical results reveal a superconducting state in the AP *Amam* phase, while the pairing strength is significantly weaker than that in the HP *I_4mmm* phase at 30 GPa. Furthermore, we simulate the influence of random oxygen vacancy configurations, demonstrating that apical oxygen vacancies act to suppress both pairing strength and superfluid density. These findings provide valuable theoretical insights into the impact of pressure and oxygen vacancies on the superconducting properties of $\text{La}_3\text{Ni}_2\text{O}_7$, offering guidance for future experimental and theoretical investigations.

Results

Effective bilayer single-orbital model

The electronic properties of $\text{La}_3\text{Ni}_2\text{O}_7$ is dominated by the two E_g orbitals [47]. Naive valence counting shows that the $3d_{z^2}$ orbital is nearly half-filled, while the $3d_{x^2-y^2}$ orbital is approximately quarter-filled. Besides, $\text{La}_3\text{Ni}_2\text{O}_7$ exhibits strong electronic correlations, as evidenced by optical measurements showing the suppression of electron kinetic energy [25] and band renormalization revealed from ARPES data [26], placing the system near a Mott-insulating phase. Under strong Hubbard repulsion, the electrons in the $3d_{z^2}$ orbital become effectively localized [26, 47], behaving as spins. SC primarily contributes from the $3d_{x^2-y^2}$ orbital, which shares similarities with the 50% hole-doped cuprates. However, the in-plane superexchange interaction between the $3d_{x^2-y^2}$ electrons alone is not sufficient to account for high- T_c SC.

A critical aspect of the pairing mechanism in $\text{La}_3\text{Ni}_2\text{O}_7$ lies in the interplay between the $3d_{z^2}$ and $3d_{x^2-y^2}$ orbitals. The strong interlayer antiferromagnetic (AFM) superexchange associated with the $3d_{z^2}$ spins is trans-

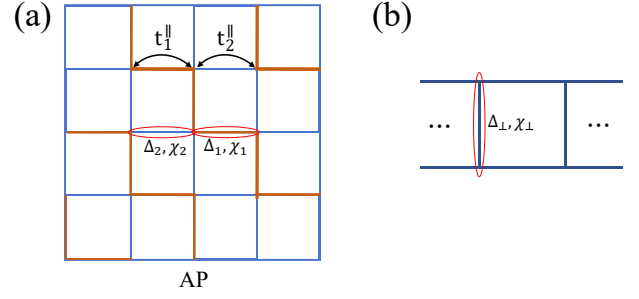


FIG. 2. (color online) (a) Schematic diagram for the intra-layer NN hopping process at AP, and the two types of intra-layer order parameters ($\Delta_{1,2}, \chi_{1,2}$). (b) Schematic diagram for the inter-layer order parameters ($\Delta_{\perp}, \chi_{\perp}$).

mitted to the $3d_{x^2-y^2}$ orbital via Hund's coupling [54]. This coupling mediates an effective interlayer spin exchange J_{\perp} between $3d_{x^2-y^2}$ spins, which is essential for the emergence of SC in this system. This scenario leads to a bilayer t - J - J_{\perp} model that captures the essential physics of the $3d_{x^2-y^2}$ orbital under strong Hund's coupling [54, 55, 57].

The minimal effective model consists of a bilayer t - J_{\parallel} - J_{\perp} Hamiltonian can be expressed as follows:

$$\begin{aligned}
 H = & \sum_{\langle i,j \rangle \alpha \sigma} -t_{\parallel}^{\langle i,j \rangle} (c_{x^2 i \alpha \sigma}^{\dagger} c_{x^2 j \alpha \sigma} + \text{h.c.}) \\
 & - t_{\perp} \sum_{i \sigma} (c_{x^2 i 1 \sigma}^{\dagger} c_{x^2 i 2 \sigma} + \text{h.c.}) \\
 & + \sum_{\langle i,j \rangle \alpha} J_{\parallel} \mathbf{S}_{x^2 i \alpha} \cdot \mathbf{S}_{x^2 j \alpha} + J_{\perp} \sum_i \mathbf{S}_{x^2 i 1} \cdot \mathbf{S}_{x^2 i 2},
 \end{aligned} \quad (1)$$

where $c_{x^2 i \alpha \sigma}^{\dagger}$ is the electron creation operator for $3d_{x^2-y^2}$ orbital at the lattice site i ; $\alpha = 1, 2$ is the layer index for the NiO_2 plane and $\sigma = \uparrow, \downarrow$ is the spin index; $\mathbf{S}_{x^2 i \alpha} = \frac{1}{2} c_{x^2 i \alpha}^{\dagger} [\boldsymbol{\sigma}] c_{x^2 i \alpha}$ is the spin operator for $3d_{x^2-y^2}$ electron, with Pauli matrices $\boldsymbol{\sigma} = (\sigma_x, \sigma_y, \sigma_z)$. The summation $\sum_{\langle i,j \rangle}$ takes over all the nearest-neighboring (NN) pair $\langle i, j \rangle$ within the NiO_2 plane. In the following study, t is set as the energy unit. The super-exchange interaction is effectively approximately as $J_{\parallel} = 4t_{\parallel}^2/U$, where U is the Hubbard interaction in the $3d_{x^2-y^2}$ orbital.

This effective $3d_{x^2-y^2}$ orbital t - J_{\parallel} - J_{\perp} model could exhibit high- T_c SC with interlayer s -wave pairing [54, 57, 67, 69, 71]. The important role of Hund's coupling for stabilizing SC has also been numerically confirmed [73, 74]. The strong interlayer AFM exchange crucial for SC has been experimentally revealed from spin excitation studies [79, 90]. We further predict element substitution could enhance the SC based on this pairing mechanism [68], consistent with recent experimental on $\text{La}_2\text{ReNi}_2\text{O}_7$ (Re:rare earth) [24, 44].

Pressure and Superconductivity

We now turn to the effect of pressure on the electronic properties. The intra-layer hopping parameters $t_{\parallel}^{\langle i,j \rangle}$ for

AP OP	GS value (eV)	HP OP	GS value (eV)
Δ_{\perp}	-2.40×10^{-3}	Δ_{\perp}	-1.38×10^{-2}
Δ_{\parallel}	7.18×10^{-6}	Δ_{\parallel}	6.83×10^{-5}
Δ_2	5.83×10^{-6}		
χ_{\perp}	1.59×10^{-3}	χ_{\perp}	2.54×10^{-3}
χ_1	1.97×10^{-2}	χ_{\parallel}	3.23×10^{-2}
χ_2	1.96×10^{-2}		
	filling		filling
x	0.25	x	0.3

TABLE I. Table of the hopping and pairing order parameters (OPs) calculated by the SBMF theory in the ground state (GS) as well as the physical electron filling x .

both types of intra-layer and inter-layer order parameters are shown in Fig. 2(a) and (b), respectively. In the AP phase, spatial inversion symmetry ensures that the inter-layer order parameters are identical within the sublattice. Density functional theory (DFT) calculations [82] provide the relevant AP hopping parameters: $t_{\parallel}^{\parallel} = 0.4025$ eV, $t_2^{\parallel} = 0.3976$ eV, $t_{xx}^{\perp} = 0.0182$ eV, and $t_{zz}^{\perp} = 0.597$ eV. Under high pressure, the hopping parameters are modified to $t^{\parallel} = 0.49$ eV, $t_{xx}^{\perp} = 0.0245$ eV, and $t_{zz}^{\perp} = 0.67$ eV. The spin superexchange J scales as t^2 in the strong coupling limit, which would also become stronger under pressure.

We apply the slave-boson mean-field (SBMF) approach [122, 123] to the bilayer t - J model to investigate the superconducting properties. For a typical Hubbard interaction value of $U = 4$ eV, the simulated order parameters at AP 0 GPa and HP 30 GPa are calculated and summarized in Table I. With increasing pressure, the superexchange coupling strengthens, leading to an increasing pairing amplitude Δ_{\perp} from 2.40×10^{-3} eV to 1.38×10^{-2} eV. Due to the larger inter-layer superexchange, the inter-layer pairing amplitude Δ_{\perp} is significantly stronger than the intra-layer one Δ_{\parallel} . Notably, Δ_{\perp} and Δ_{\parallel} possess opposite signs, a feature reminiscent of d -wave pairing symmetry when viewed from the side. This sign difference highlights the complex nature of the pairing symmetry in this system.

The filling-dependent pairing strengths for AP 0 GPa and HP 30 GPa are shown in Fig. 3(a), where the inter-layer pairing amplitudes Δ_{\perp} grow as the filling level increases. The increase in Δ_{\perp} indicates a corresponding rise in the transition temperature T_c . At finite temperatures, T_c can be estimated by the point where Δ_{\perp} vanishes. The numerical simulation of T_c is shown in Fig. 3(b), where from 0 GPa to 30 GPa at physical filling level 0.25, T_c increases dramatically from 15 K to 87 K. Our calculations also give a ratio of $\Delta_{\perp}/T_c \approx 1.6$, consistent with the predictions of BCS theory.

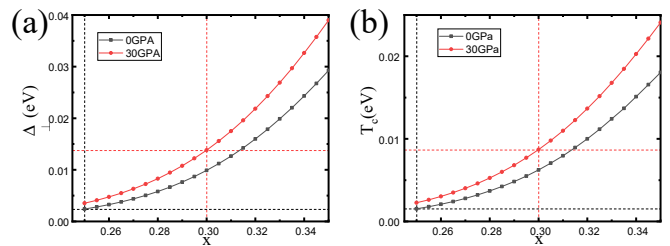


FIG. 3. (color online) (a) Inter-layer pairing gap Δ_{\perp} versus filling level x . (b) Superconducting T_c versus filling level x . The place of AP (HP) physical filling $x = 0.25$ ($x = 0.3$) is shown in a black (red) dashed line.

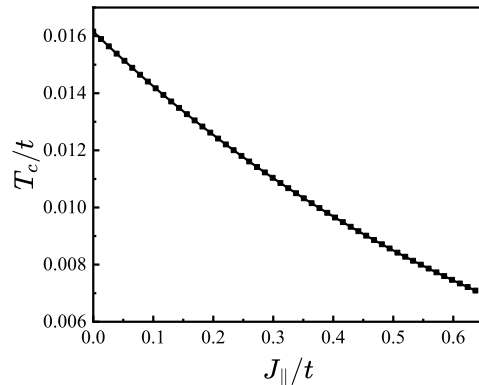


FIG. 4. T_c versus intralayer superexchange J_{\parallel} , at $J_{\perp} = 0.8t$, $x = 0.3$.

Most experimental data have suggested that there is no bulk SC in the AP phase [19–24]. The suppression of SC at ambient pressure can be attributed to two main factors: First, ARPES experimental [26] and DFT calculations [47] both reveal that in the AP phase, the $3d_{z^2}$ orbital is exactly below the Fermi surface and will not contribute to the electronic property. The electron filling of the $3d_{x^2-y^2}$ orbital is well-approximated by quarter-filling, which is significantly over-doped and itinerant, reducing its electronic correlations and, consequently, the pairing interactions. Second, at AP A_{1g} phase, the inter-layer hopping of the $3d_{z^2}$ orbital is quite small, leading to a significant reduction in the inter-layer superexchange interaction J_{\perp} , further diminishing the pairing strength.

DFT calculations [53] also show that further increasing pressure decreases the ratio of the inter-layer NN hopping for the $3d_{z^2}$ orbital to the intra-layer NN hopping for the $3d_{x^2-y^2}$ orbital. This change directly affects the antiferromagnetic superexchange coupling J , which scales as $4t^2/U$ in the strong-coupling limit. As a result, the ratio of inter-layer to intra-layer exchange couplings, J_{\perp}/J_{\parallel} , decreases under pressure. Further studies indicate that the superconducting T_c depends exponentially on the ratio J_{\perp}/J_{\parallel} : as J_{\perp}/J_{\parallel} increases, T_c rises sharply, and conversely, it drops quickly as J_{\perp}/J_{\parallel} decreases [54].

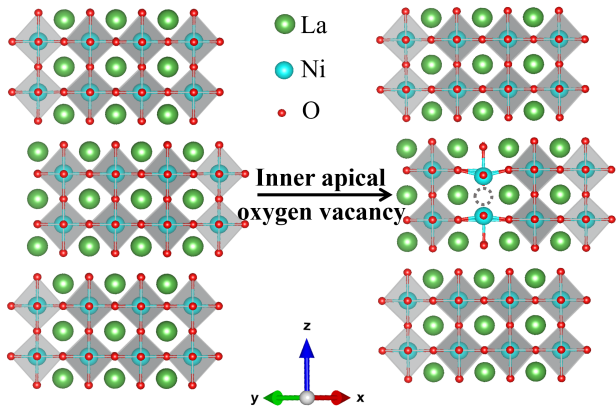


FIG. 5. (color online) Structural comparison between pristine $\text{La}_3\text{Ni}_2\text{O}_7$ and $\text{La}_3\text{Ni}_2\text{O}_{7-\delta}$, projected along the $[110]$ axis. The left diagram displays the regular lattice structure of $\text{La}_3\text{Ni}_2\text{O}_7$, composed of alternating layers of NiO_2 and LaO planes. The right diagram illustrates $\text{La}_3\text{Ni}_2\text{O}_{7-\delta}$ with an oxygen vacancy at the inner apical position, marked by a black dashed circle.

This suggests that the observed reduction in T_c at higher pressures can be attributed to the reduction of J_{\perp}/J_{\parallel} .

To further illustrate this phenomenon, we performed additional test employing the effective single-orbital t - J model. As shown in Fig. 4, we fixed the hopping amplitude t , the inter-layer exchange coupling J_{\perp} , and the filling level while systematically increasing intra-layer coupling J_{\parallel} . The results show a rapid decrease in T_c , revealing the competition between interlayer and intralayer pairing channels. These findings strongly suggest that the suppression of T_c under higher pressure [120] is driven by the delicate balance between interlayer and intralayer exchange couplings. Upon further compression, the hybridization V between orbitals might become increasingly significant, potentially leading to a suppression of T_c to zero [61, 73].

Oxygen Vacancies and Superconductivity

The inter-layer apical oxygen, positioned between the two Ni-O layers, plays a critical role for the SC of $\text{La}_3\text{Ni}_2\text{O}_7$ [19, 49, 85, 89, 120, 121]. Experimental direct visualization studies suggest that the apical oxygen is particularly prone to vacancy formation [42, 120]. The schematic crystal structure, presented in Fig. 5, illustrates the system with apical oxygen vacancies. The removal of apical oxygen atoms induces substantial local structural distortions, reducing the NiO_6 octahedra into NiO_5 pyramids. These distortions significantly alter the symmetry of the local crystal structure, resulting in anisotropic lattice constant changes: a marked contraction along the c -axis, accompanied by a slighter expansion of the in-plane lattice constants (a and b). These structural modifications are expected to further influence both intralayer and interlayer electron hopping, as well as orbital hybridization. To maintain generality and clarity,

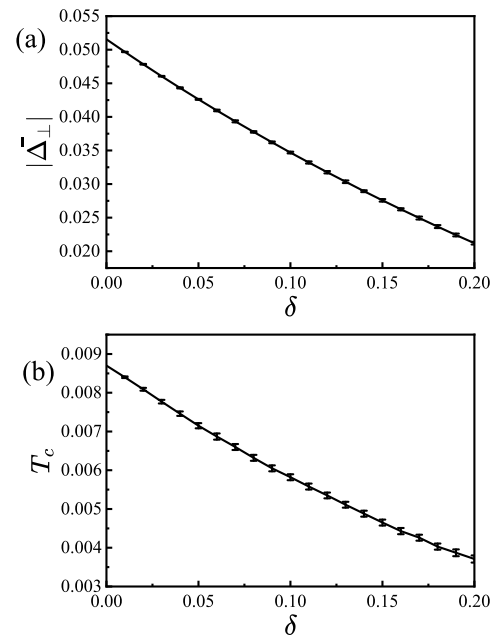


FIG. 6. Dependence of pairing order parameters and superconducting T_c on apical-oxygen vacancy concentrations δ . (a) Dependence of pairing order parameters perpendicular to the Ni-O plane Δ_{\perp} on δ . (b) Dependence of superconducting T_c on δ . Note that for each δ , we randomly computed results for 100 samples. The solid line represents the distribution of mean values, while the error bars are the standard deviation of the deviation of each sample's data from the mean.

we normalize the energy scales by setting $t_{\parallel} = 1$, $J_{\parallel} = 0.4$ and $J_{\perp} = 0.8$.

We first compute the effects of apical oxygen vacancies on the ground state SC pairing. Interlayer pairing strength Δ_{\perp} remains as the dominate pairing channel. The averaged Δ_{\perp} is depicted in Fig. 6, which is significantly reduced as the concentration of apical oxygen vacancies increases. Fig. 7(a), (d) and (g) further displays the pairing order parameters for various random configurations at oxygen vacancy concentrations of $\delta = 5\%$, 10% , 15% . It is evident that, due to the breaking of Ni-O-Ni bonds, Δ_{\perp} vanishes locally at defect sites. Additionally, the results highlight how Δ_{\perp} is progressively suppressed in the vicinity of these vacancies, with the suppression intensifying as δ rises. A similar pattern of suppression is also observed for the in-plane pairing Δ_{\parallel} , as shown in Fig. 7 (b), (e), and (h).

The suppression of SC near oxygen vacancies is closely related to the reduction of electronic density of states. At the vacancy site, the interlayer Ni-O-Ni bond is disrupted, reducing the electronic itinerancy and increasing the on-site energy of electrons at this location. Consequently, the local electron density around the apical oxygen vacancy decreases, as directly illustrated in Fig. 7 (c), (f), and (i). According to BCS theory, the superconducting gap Δ and critical temperature T_c scales as

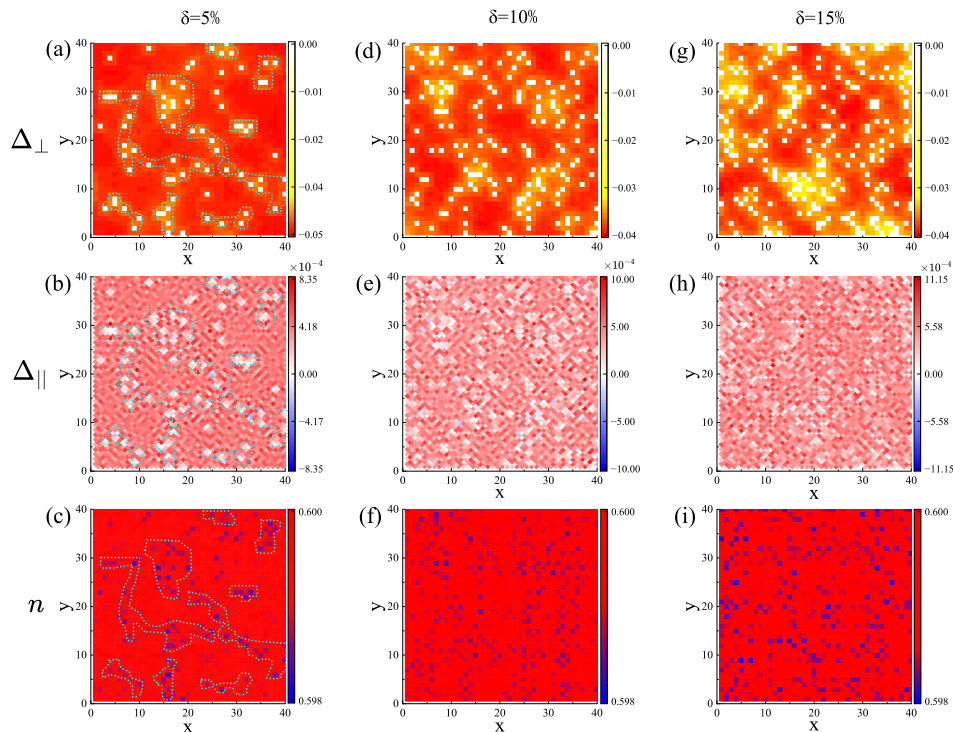


FIG. 7. (color online) Spatial distributions of the pairing order parameters Δ_{\perp} (perpendicular to the Ni-O plane) and Δ_{\parallel} (parallel to the Ni-O plane), along with the particle number density n , for different apical-oxygen vacancy concentrations δ . The top row (a,d,g) shows the distribution of Δ_{\perp} , the middle row (b,e,h) presents the distribution of Δ_{\parallel} , and the bottom row (c,f,i) illustrates the spatial distribution of n . The columns correspond to different apical-oxygen vacancy concentrations: the first column (a)-(c) for $\delta = 5\%$, the second column (d)-(f) for $\delta = 10\%$, and the third column (g)-(i) for $\delta = 15\%$. Color bars indicate the magnitude of each quantity, highlighting variations caused by oxygen vacancy in superconducting properties and charge distribution. Note that for each δ , we randomly computed results for 100 samples, and the presented findings here correspond to one randomly selected configuration.

$\propto \exp(\frac{1}{N_F V_{eff}})$, where N_F is the density of states near the Fermi level, and V_{eff} is the effective interaction strength. Therefore, the reduction in electronic density of states near the vacancies results in a weakening of the pairing strength. Additionally, as detailed in the supplementary, the distribution of the hopping order parameter χ at various vacancy concentrations exhibits a trend similar to that of Δ , further reinforcing this observation.

The dependence of the T_c on the concentration of apical oxygen vacancies δ , calculated using the finite-temperature SBMF framework, is presented in Fig. 6 (b). The variation in T_c consistently follows the behavior of Δ_{\perp} , underscoring the critical role that apical oxygen vacancies play in stabilizing the SC of $\text{La}_3\text{Ni}_2\text{O}_7$ under pressure.

In addition, we explored the impact of different oxygen vacancy concentrations on the superfluid density. As shown in Fig. 8, the superfluid density decreases rapidly with the increasing in apex oxygen vacancies. This phenomenon arises from two primary factors. On the one hand, the apical oxygen vacancies reduce the superconducting pairing strength and simultaneously decrease the diamagnetic current density. On the other

hand, the presence of oxygen vacancies introduces randomness, which significantly enhances the paramagnetic current density. Consequently, the decrease in diamagnetic current density coupled with the increase in paramagnetic current density inevitably leads to a reduction

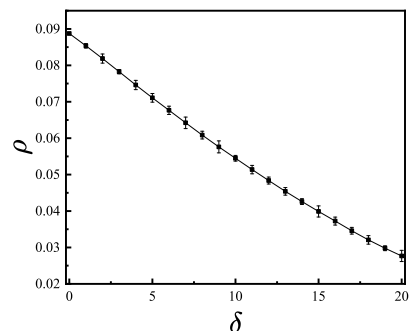


FIG. 8. Dependence of superfluid density ρ on apical-oxygen vacancy concentrations δ . Note that for each δ , we randomly computed results for 100 samples. The solid line represents the distribution of mean values, while the error bars are the standard deviation of the deviation of each sample's data from the mean.

in the superfluid density. This result is consistent with experimental measurements, which show a significantly reduced diamagnetic fraction in samples with a higher concentration of apical oxygen vacancies [29].

Discussion In summary, we have employed the SBMF method to investigate the effects of pressure and apical oxygen vacancies on the SC of $\text{La}_3\text{Ni}_2\text{O}_7$. The results show that the SC exhibits a right-triangle dependence versus pressure and temperature. In the optimal HP phase at 30 GPa, the pairing strength is enhanced greater than in the AP phase at 0 GPa. Then, the superconducting critical T_c decreases as pressure continues to increase, suggesting that excessive pressure may eventually suppress SC. We further investigated the influence of apical oxygen vacancies on SC by simulating the problem within the randomness in real space. The introduction of apical oxygen vacancies significantly weakens SC, a suppression that is also evident in the calculated pairing order parameters and density distributions. These results align with experimental observations of extremely weak diamagnetic signals in many samples, particularly those with high concentrations of oxygen vacancies.

Recent experiments on bulk $\text{La}_3\text{Ni}_2\text{O}_7$ at AP show signatures of high- T_c SC at 80 K, albeit with a low volume fraction ($\sim 0.2\%$) [45]. This is consistent with a filamentary SC scenario at AP, suggested by the weak diamagnetic response likely originating from strained boundaries. Conversely, resistivity data reveals a broad resistance drop near 20 K, followed by a plateau at lower temperatures [45], hinting at a bulk-like SC phase at AP. Interestingly, this lower temperature is close to the theoretical predictions of weak SC around 15 K in this work (e.g., Fig. 3(b)). Thus, experimental data at AP [45] might be attributed as: the 80 K signature from diamagnetism indicates filamentary SC at strained boundaries, while the 20 K resistivity plateau suggests a weaker, bulk SC phase.

Overall, our findings provide a theoretical explanation for the experimentally observed pressure dependence of SC, including the enhancement of SC under moderate pressure and its suppression by apical oxygen vacancies. These insights deepen our understanding of the delicate interplay between structural factors and SC in this bilayer nickelate system. Moreover, the perspective under AP phase points to a potential realization of AP SC in the bulk material.

Methods

Slave-boson mean-field theory

In the slave-boson mean field theory, the $3d_{x^2-y^2}$ -orbital electron operator is expressed as $c_{i\alpha\sigma}^\dagger = f_{i\alpha\sigma}^\dagger b_{i\alpha}$, where $f_{i\alpha\sigma}^\dagger/b_{i\alpha}$ is the spinon/holon creation/annihilation operator, with the local constraint $\sum_\sigma f_{i\alpha\sigma}^\dagger f_{i\alpha\sigma} + b_{i\alpha}^\dagger b_{i\alpha} = 1$. Introduce the intra-layer hoppings and pair-

ings ones,

$$\begin{aligned}\chi_{ij}^{(\alpha)} &= f_{j\alpha\uparrow}^\dagger f_{i\alpha\uparrow} + f_{j\alpha\downarrow}^\dagger f_{i\alpha\downarrow}, \\ \Delta_{ij}^{(\alpha)} &= f_{j\alpha\downarrow}^\dagger f_{i\alpha\uparrow} - f_{j\alpha\uparrow}^\dagger f_{i\alpha\downarrow}\end{aligned}\quad (2)$$

and the interlayer hoppings and pairings ones,

$$\begin{aligned}\chi_{i,\perp} &= f_{i2\uparrow}^\dagger f_{i1\uparrow} + f_{i2\downarrow}^\dagger f_{i1\downarrow}, \\ \Delta_{i,\perp} &= f_{i2\downarrow}^\dagger f_{i1\uparrow} - f_{i2\uparrow}^\dagger f_{i1\downarrow},\end{aligned}\quad (3)$$

The holon will condense at low temperature and holon operator can be replaced by its condensation density below the condensation temperature, $b_{i\alpha} \sim b_{i\alpha}^\dagger \sim \sqrt{\delta} = \sqrt{1-2x}$, where $x \sim 0.3$ represents the electron filling of the $d_{x^2-y^2}$ -orbital under pressure-induced self-doping effects[60].

The spin superexchange can be decoupled in the hopping and pairing channel, i.e., for the inter-layer one,

$$\begin{aligned}J_\perp \mathbf{S}_{x^2i1} \cdot \mathbf{S}_{x^2i2} \\ = - \left[\chi_{i\perp} (f_{i1\uparrow}^\dagger f_{i2\uparrow} + f_{i1\downarrow}^\dagger f_{i2\downarrow}) + \text{h.c.} - \frac{8|\chi_{i\perp}|^2}{3J_\perp} \right] \\ - \left[\Delta_{i\perp} (f_{i1\uparrow}^\dagger f_{i2\downarrow} - f_{i1\downarrow}^\dagger f_{i2\uparrow}) + \text{h.c.} - \frac{8|\Delta_{i\perp}|^2}{3J_\perp} \right],\end{aligned}\quad (4)$$

In the mean-field analysis, hoppings χ , pairings Δ and Lagrange multipliers $\lambda_{i\alpha}$ are replaced by their site-independent mean-field values,

$$\begin{aligned}\chi_{ij}^{(\alpha)} &= \frac{3}{8} J_\parallel \langle f_{j\alpha\uparrow}^\dagger f_{i\alpha\uparrow} + f_{j\alpha\downarrow}^\dagger f_{i\alpha\downarrow} \rangle \equiv \chi_{j-i}^{(\alpha)}, \\ \Delta_{ij}^{(\alpha)} &= \frac{3}{8} J_\parallel \langle f_{j\alpha\downarrow}^\dagger f_{i\alpha\uparrow} - f_{j\alpha\uparrow}^\dagger f_{i\alpha\downarrow} \rangle \equiv \Delta_{j-i}^{(\alpha)}, \\ \chi_{i\perp} &= \frac{3}{8} J_\perp \langle f_{i2\uparrow}^\dagger f_{i1\uparrow} + f_{i2\downarrow}^\dagger f_{i1\downarrow} \rangle \equiv \chi_\perp, \\ \Delta_{i\perp} &= \frac{3}{8} J_\perp \langle f_{i2\downarrow}^\dagger f_{i1\uparrow} - f_{i2\uparrow}^\dagger f_{i1\downarrow} \rangle \equiv \Delta_\perp.\end{aligned}\quad (5)$$

The mean-field Hamiltonian for the spinon part is given by,

$$\begin{aligned}H_{f,\text{MF}} &= \sum_{\mathbf{k}\alpha\sigma} \varepsilon_{\mathbf{k},\alpha} f_{\mathbf{k}\alpha\sigma}^\dagger f_{\mathbf{k}\alpha\sigma} \\ &- \sum_{\mathbf{k}} \left[\left(\frac{3}{8} J_\perp \chi_z + t_\perp \delta \right) (f_{\mathbf{k}1\uparrow}^\dagger f_{\mathbf{k}2\uparrow} + f_{-\mathbf{k}1\downarrow}^\dagger f_{-\mathbf{k}2\downarrow}) + \text{h.c.} \right] \\ &+ \sum_{\mathbf{k}\alpha} (F_{\mathbf{k},\alpha} f_{\mathbf{k}\alpha\uparrow}^\dagger f_{-\mathbf{k}\alpha\downarrow}^\dagger + \text{h.c.}) \\ &- \frac{3}{8} J_\parallel \sum_{\mathbf{k}} \Delta_z \left[(f_{\mathbf{k}1\uparrow}^\dagger f_{-\mathbf{k}2\downarrow}^\dagger - f_{-\mathbf{k}1\downarrow}^\dagger f_{\mathbf{k}2\uparrow}^\dagger) + \text{h.c.} \right] \\ &- \frac{3}{8} J_\parallel N \sum_{\alpha} (|\chi_x^{(\alpha)}|^2 + |\chi_y^{(\alpha)}|^2 + |\Delta_x^{(\alpha)}|^2 + |\Delta_y^{(\alpha)}|^2) \\ &+ \frac{3}{8} J_\perp N (|\chi_\perp|^2 + |\Delta_\perp|^2)\end{aligned}\quad (6)$$

where the intralayer kinetic energy and pairing are,

$$\begin{aligned}\varepsilon_{\mathbf{k},\alpha} &= -\frac{3}{8}J_{\parallel}[\chi_x^{(\alpha)}e^{-ik_x} + \chi_y^{(\alpha)}e^{-ik_y} + \text{h.c.}] \\ &\quad - 2t\delta[\cos k_x + \cos k_y] - \mu_f, \\ F_{\mathbf{k},\alpha} &= -\frac{3}{4}J_{\parallel}[\Delta_x^{(\alpha)}\cos k_x + \Delta_y^{(\alpha)}\cos k_y],\end{aligned}\quad (7)$$

and μ_f is the chemical potential of the spinon field.

Date availability

Relevant data supporting the key findings of this study are available within the article and the Supplementary Information file. All raw data generated during the current study are available from the corresponding authors upon request.

Code availability

The code that supports the plots within this paper is available from the corresponding author upon request.

* These three authors contributed equally to this work.

† yangfan_blg@bit.edu.cn

- [1] S. Taniguchi, T. Nishikawa, Y. Yasui, Y. Kobayashi, J. Takeda, S.-i. Shamoto, and M. Sato, Transport, magnetic and thermal properties of $\text{La}_3\text{Ni}_2\text{O}_{7-\delta}$, *J. Phys. Soc. Jpn.* **64**, 1644 (1995).
- [2] D.-K. Seo, W. Liang, M.-H. Whangbo, Z. Zhang, and M. Greenblatt, Electronic band structure and madelung potential study of the nickelates La_2NiO_4 , $\text{La}_3\text{Ni}_2\text{O}_7$, and $\text{La}_4\text{Ni}_3\text{O}_{10}$, *Inorg. Chem.* **35**, 6396 (1996).
- [3] Y. Kobayashi, S. Taniguchi, M. Kasai, M. Sato, T. Nishioka, and M. Kontani, Transport and magnetic properties of $\text{La}_3\text{Ni}_2\text{O}_{7-\delta}$ and $\text{La}_4\text{Ni}_3\text{O}_{10-\delta}$, *J. Phys. Soc. Jpn.* **65**, 3978 (1996).
- [4] M. Greenblatt, Ruddlesden-popper $\text{Ln}_{n+1}\text{Ni}_n\text{O}_{3n+1}$ nickelates: structure and properties, *Curr. Opin. Solid State Mater. Sci.* **2**, 174 (1997).
- [5] M. Greenblatt, Z. Zhang, and M. Whangbo, Electronic properties of $\text{La}_3\text{Ni}_2\text{O}_7$ and $\text{La}_4\text{Ni}_3\text{O}_{10}$, $\text{Ln}=\text{La}, \text{Pr}$ and Nd , *Synth. Met.* **85**, 1451 (1997).
- [6] C. D. Ling, D. N. Argyriou, G. Wu, and J. Neumeier, Neutron diffraction study of $\text{La}_3\text{Ni}_2\text{O}_7$: Structural relationships among $n=1,2$, and 3 phases $\text{La}_{n+1}\text{Ni}_n\text{O}_{3n+1}$, *J. Solid State Chem.* **152**, 517 (2000).
- [7] G. Wu, J. J. Neumeier, and M. F. Hundley, Magnetic susceptibility, heat capacity, and pressure dependence of the electrical resistivity of $\text{La}_3\text{Ni}_2\text{O}_7$ and $\text{La}_4\text{Ni}_3\text{O}_{10}$, *Phys. Rev. B* **63**, 245120 (2001).
- [8] T. Fukamachi, Y. Kobayashi, T. Miyashita, and M. Sato, ^{139}La NMR studies of layered perovskite systems $\text{La}_3\text{Ni}_2\text{O}_{7-\delta}$ and $\text{La}_4\text{Ni}_3\text{O}_{10}$, *J. Phys. Chem. Solids* **62**, 195 (2001).
- [9] V. I. Voronin, I. F. Berger, V. A. Cherepanov, L. Y. Gavrilova, A. N. Petrov, A. I. Ancharov, B. Tolochko, and S. G. Nikitenko, Neutron diffraction, synchrotron radiation and exafs spectroscopy study of crystal structure peculiarities of the lanthanum nickelates $\text{La}_{n+1}\text{Ni}_n\text{O}_y$ ($n=1,2,3$), *Nucl. Instrum. Methods Phys. Res. A* **470**, 202 (2001).
- [10] D. O. Bannikov, A. P. Safronov, and V. A. Cherepanov, Thermochemical characteristics of $\text{La}_{n+1}\text{Ni}_n\text{O}_{3n+1}$ oxides, *Thermochim. Acta* **451**, 22 (2006).
- [11] T. Hosoya, K. Igawa, Y. Takeuchi, K. Yoshida, T. Uryu, H. Hirabayashi, and H. Takahashi, Pressure studies on the electrical properties in $\text{R}_{2-x}\text{Sr}_x\text{Ni}_{1-y}\text{Cu}_y\text{O}_{4+\delta}$ ($\text{R}=\text{La}, \text{Nd}$) and $\text{La}_3\text{Ni}_2\text{O}_{7+\delta}$, *J. Phys.: Conf. Ser.* **121**, 052013 (2008).
- [12] V. Pardo and W. E. Pickett, Metal-insulator transition in layered nickelates $\text{La}_3\text{Ni}_2\text{O}_{7-\delta}$ ($\delta=0.0, 0.5, 1$), *Phys. Rev. B* **83**, 245128 (2011).
- [13] M. Nakata, D. Ogura, H. Usui, and K. Kuroki, Finite-energy spin fluctuations as a pairing glue in systems with coexisting electron and hole bands, *Phys. Rev. B* **95**, 214509 (2017).
- [14] Y. Mochizuki, H. Akamatsu, Y. Kumagai, and F. Oba, Strain-engineered peierls instability in layered perovskite $\text{La}_3\text{Ni}_2\text{O}_7$ from first principles, *Phys. Rev. Mater.* **2**, 125001 (2018).
- [15] Z. Li, W. Guo, T. T. Zhang, J. H. Song, T. Y. Gao, Z. B. Gu, and Y. F. Nie, Epitaxial growth and electronic structure of ruddlesden-popper nickelates ($\text{La}_{n+1}\text{Ni}_n\text{O}_{3n+1}$, $n=1-5$), *APL Mater.* **8**, 091112 (2020).
- [16] J. Song, D. Ning, B. Boukamp, J.-M. Bassat, and H. J. Bouwmeester, Structure, electrical conductivity and oxygen transport properties of ruddlesden-popper phases $\text{Ln}_{n+1}\text{Ni}_n\text{O}_{3n+1}$ ($\text{Ln}=\text{La}, \text{Pr}$ and Nd ; $n=1, 2$ and 3), *J. Mater. Chem. A* **8**, 22206 (2020).
- [17] M. R. Barone, N. M. Dawley, H. P. Nair, B. H. Goodge, M. E. Holtz, A. Soukiasian, E. E. Fleck, K. Lee, Y. Jia, T. Heeg, R. Gatt, Y. Nie, D. A. Muller, L. F. Kourkoutis, and D. G. Schlom, Improved control of atomic layering in perovskite-related homologous series, *APL Mater.* **9**, 021118 (2021).
- [18] Z. Liu, H. Sun, M. Huo, X. Ma, Y. Ji, E. Yi, L. Li, H. Liu, J. Yu, Z. Zhang, Z. Chen, F. Liang, H. Dong, H. Guo, D. Zhong, B. Shen, S. Li, and M. Wang, Evidence for charge and spin density waves in single crystals of $\text{La}_3\text{Ni}_2\text{O}_7$ and $\text{La}_3\text{Ni}_2\text{O}_6$, *Sci. China-Phys. Mech. Astron.* **66**, 217411 (2023).
- [19] H. Sun, M. Huo, X. Hu, J. Li, Z. Liu, Y. Han, L. Tang, Z. Mao, P. Yang, B. Wang, J. Cheng, D.-X. Yao, G.-M. Zhang, and M. Wang, Signatures of superconductivity near 80K in a nickelate under high pressure, *Nature* **621**, 493 (2023).
- [20] J. Hou, P.-T. Yang, Z.-Y. Liu, J.-Y. Li, P.-F. Shan, L. Ma, G. Wang, N.-N. Wang, H.-Z. Guo, J.-P. Sun, Y. Uwatoko, M. Wang, G.-M. Zhang, B.-S. Wang, and J.-G. Cheng, Emergence of high-temperature superconducting phase in pressurized $\text{La}_3\text{Ni}_2\text{O}_7$ crystals, *Chin. Phys. Lett.* **40**, 117302 (2023).
- [21] Y. Zhang, D. Su, Y. Huang, Z. Shan, H. Sun, M. Huo, K. Ye, J. Zhang, Z. Yang, Y. Xu, Y. Su, R. Li, M. Smidman, M. Wang, L. Jiao, and H. Yuan, High-temperature superconductivity with zero resistance and strange-metal behaviour in $\text{La}_3\text{Ni}_2\text{O}_{7-\delta}$, *Nat. Phys.* **20**, 1269 (2024).
- [22] G. Wang, N. N. Wang, X. L. Shen, J. Hou, L. Ma, L. F. Shi, Z. A. Ren, Y. D. Gu, H. M. Ma, P. T. Yang, Z. Y. Liu, H. Z. Guo, J. P. Sun, G. M. Zhang, S. Calder, J.-Q. Yan, B. S. Wang, Y. Uwatoko, and J.-G. Cheng, Pressure-induced superconductivity in polycrystalline $\text{La}_3\text{Ni}_2\text{O}_7$, *Phys. Rev. X* **14**, 011040 (2024).

- [23] G. Wang, N. Wang, Y. Wang, L. Shi, X. Shen, J. Hou, H. Ma, P. Yang, Z. Liu, H. Zhang, X. Dong, J. Sun, B. Wang, K. Jiang, J. Hu, Y. Uwatoko, and J. Cheng, Observation of high-temperature superconductivity in the high-pressure tetragonal phase of $\text{La}_2\text{PrNi}_2\text{O}_{7-\delta}$, [arXiv:2311.08212 \(2023\)](#).
- [24] N. Wang, G. Wang, X. Shen, J. Hou, J. Luo, X. Ma, H. Yang, L. Shi, J. Dou, J. Feng, J. Yang, Y. Shi, Z. Ren, H. Ma, P. Yang, Z. Liu, Y. Liu, H. Zhang, X. Dong, Y. Wang, K. Jiang, J. Hu, S. Calder, J. Yan, J. Sun, B. Wang, R. Zhou, Y. Uwatoko, and J. Cheng, Bulk high-temperature superconductivity in the high-pressure tetragonal phase of bilayer $\text{La}_2\text{PrNi}_2\text{O}_7$, [Nature **634**, 579 \(2024\)](#).
- [25] Z. Liu, M. Huo, J. Li, Q. Li, Y. Liu, Y. Dai, X. Zhou, J. Hao, Y. Lu, M. Wang, and H.-H. Wen, Electronic correlations and partial gap in the bilayer nickelate $\text{La}_3\text{Ni}_2\text{O}_7$, [Nat. Commun. **15**, 7570 \(2024\)](#).
- [26] J. Yang, H. Sun, X. Hu, Y. Xie, T. Miao, H. Luo, H. Chen, B. Liang, W. Zhu, G. Qu, C.-Q. Chen, M. Huo, Y. Huang, S. Zhang, F. Zhang, F. Yang, Z. Wang, Q. Peng, H. Mao, G. Liu, Z. Xu, T. Qian, D.-X. Yao, M. Wang, L. Zhao, and X. J. Zhou, Orbital-dependent electron correlation in double-layer nickelate $\text{La}_3\text{Ni}_2\text{O}_7$, [Nat. Commun. **15**, 4373 \(2024\)](#).
- [27] M. Zhang, C. Pei, Q. Wang, Y. Zhao, C. Li, W. Cao, S. Zhu, J. Wu, and Y. Qi, Effects of pressure and doping on ruddlesden-popper phases $\text{La}_{n+1}\text{Ni}_n\text{O}_{3n+1}$, [J. Mater. Res. Technol. **185**, 147 \(2024\)](#).
- [28] L. Wang, Y. Li, S.-Y. Xie, F. Liu, H. Sun, C. Huang, Y. Gao, T. Nakagawa, B. Fu, B. Dong, *et al.*, Structure responsible for the superconducting state in $\text{La}_3\text{Ni}_2\text{O}_7$ at high-pressure and low-temperature conditions, [J. Am. Chem. Soc. **146**, 7506 \(2024\)](#).
- [29] Y. Zhou, J. Guo, S. Cai, H. Sun, C. Li, J. Zhao, P. Wang, J. Han, X. Chen, Y. Chen, *et al.*, Investigations of key issues on the reproducibility of high- t_c superconductivity emerging from compressed $\text{La}_3\text{Ni}_2\text{O}_7$, [Matter and Radiation at Extremes **10** \(2025\)](#).
- [30] T. Cui, S. Choi, T. Lin, C. Liu, G. Wang, N. Wang, S. Chen, H. Hong, D. Rong, Q. Wang, *et al.*, Strain-mediated phase crossover in ruddlesden–popper nickelates, [Commun. Mater. **5**, 32 \(2024\)](#).
- [31] Z. Dan, Y. Zhou, M. Huo, Y. Wang, L. Nie, M. Wang, T. Wu, and X. Chen, Spin-density-wave transition in double-layer nickelate $\text{La}_3\text{Ni}_2\text{O}_7$, [arXiv:2402.03952 \(2024\)](#).
- [32] S. N. Abadi, K.-J. Xu, E. G. Lomeli, P. Puphal, M. Isobe, Y. Zhong, A. V. Fedorov, S.-K. Mo, M. Hashimoto, D.-H. Lu, B. Moritz, B. Keimer, T. P. Devereaux, M. Hepting, and Z.-X. Shen, Electronic structure of the alternating monolayer-trilayer phase of $\text{La}_3\text{Ni}_2\text{O}_7$, [arXiv:2402.07143 \(2024\)](#).
- [33] Y. D. Li, Y. T. Cao, L. Y. Liu, P. Peng, H. Lin, C. Y. Pei, M. X. Zhang, H. Wu, X. Du, W. X. Zhao, K. Y. Zhai, J. K. Zhao, M. L. Lin, P. H. Tan, Y. P. Qi, G. Li, H. J. Guo, L. Yang, and L. X. Yang, Ultrafast dynamics of bilayer and trilayer nickelate superconductors, [arXiv:2403.05012 \(2024\)](#).
- [34] Y. Li, X. Du, Y. Cao, C. Pei, M. Zhang, W. Zhao, K. Zhai, R. Xu, Z. Liu, Z. Li, *et al.*, Electronic correlation and pseudogap-like behavior of high-temperature superconductor $\text{La}_3\text{Ni}_2\text{O}_7$, [Chin. Phys. Lett. **41**, 087402 \(2024\)](#).
- [35] H.-Y. Zhang, Y.-J. Bai, F.-J. Kong, X.-Q. Wu, Y.-H. Xing, and N. Xu, Doping evolution of the normal state magnetic excitations in pressurized $\text{La}_3\text{Ni}_2\text{O}_7$, [New J. Phys. **26**, 123027 \(2024\)](#).
- [36] X. Ren, R. Sutarto, X. Wu, J. Zhang, H. Huang, T. Xiang, J. Hu, R. Comin, X. Zhou, and Z. Zhu, Resolving the electronic ground state of $\text{La}_3\text{Ni}_2\text{O}_{7-\delta}$ films, [Commun. Phys. **8**, 52 \(2025\)](#).
- [37] M. Li, Y. Wang, C. Pei, M. Zhang, N. Li, J. Guan, M. Amboage, N. Adama, Q. Kong, Y. Qi, *et al.*, Distinguishing electronic band structure of single-layer and bilayer ruddlesden-popper nickelates probed by in-situ high pressure x-ray absorption near-edge spectroscopy, [arXiv:2410.04230 \(2024\)](#).
- [38] X. Zhou, W. He, Z. Zhou, K. Ni, M. Huo, D. Hu, Y. Zhu, E. Zhang, Z. Jiang, S. Zhang, *et al.*, Revealing nanoscale structural phase separation in $\text{La}_3\text{Ni}_2\text{O}_{7-\delta}$ single crystal via scanning near-field optical microscopy, [arXiv:2410.06602 \(2024\)](#).
- [39] B. Su, C. Huang, J. Zhao, M. Huo, J. Luo, M. Wang, and Z.-G. Chen, Strongly anisotropic charge dynamics in $\text{La}_3\text{Ni}_2\text{O}_7$ with coherent-to-incoherent crossover of interlayer charge dynamics, [arXiv:2411.10786 \(2024\)](#).
- [40] E. Mijit, P. Ma, C. J. Sahle, A. D. Rosa, Z. Hu, F. De Angelis, A. Lopez, S. Amatori, G. Tchoudinov, Y. Joly, *et al.*, Local electronic properties of $\text{La}_3\text{Ni}_2\text{O}_7$ under pressure, [arXiv:2412.08269 \(2024\)](#).
- [41] B. Chen, H. Zhang, J. Li, D. Hu, M. Huo, S. Wang, C. Xi, Z. Wang, H. Sun, M. Wang, *et al.*, Unveiling the multiband metallic nature of the normal state in nickelate $\text{La}_3\text{Ni}_2\text{O}_7$, [arXiv:2412.09375 \(2024\)](#).
- [42] Z. Dong, M. Huo, J. Li, J. Li, P. Li, H. Sun, L. Gu, Y. Lu, M. Wang, Y. Wang, and Z. Chen, Visualization of oxygen vacancies and self-doped ligand holes in $\text{La}_3\text{Ni}_2\text{O}_{7-\delta}$, [Nature **630**, 847 \(2024\)](#).
- [43] M. Shi, D. Peng, Y. Li, Z. Xing, Y. Wang, K. Fan, H. Li, R. Wu, Z. Zeng, Q. Zeng, *et al.*, Prerequisite of superconductivity: Sdw rather than tetragonal structure in double-layer $\text{La}_3\text{Ni}_2\text{O}_{7-x}$, [arXiv:2501.14202 \(2025\)](#).
- [44] F. Li, D. Peng, J. Dou, N. Guo, L. Ma, C. Liu, L. Wang, Y. Zhang, J. Luo, J. Yang, *et al.*, Ambient pressure growth of bilayer nickelate single crystals with superconductivity over 90 k under high pressure, [arXiv:2501.14584 \(2025\)](#).
- [45] M. Huo, P. Ma, C. Huang, X. Huang, H. Sun, and M. Wang, Low volume fraction of high- t_c superconductivity in $\text{La}_3\text{Ni}_2\text{O}_7$ at 80 k and ambient pressure, [arXiv:2501.15929 \(2025\)](#).
- [46] Y. Zhang, C. Pei, N. Guo, L. Fan, M. Zhang, L. Wang, G. Zhang, F. Li, Y. Wang, C. Ma, *et al.*, Damage of bilayer structure in $\text{La}_3\text{Ni}_2\text{O}_{7-\delta}$ induced by high po2 annealing, [arXiv:2502.01501 \(2025\)](#).
- [47] Z. Luo, X. Hu, M. Wang, W. Wú, and D.-X. Yao, Bilayer two-orbital model of $\text{La}_3\text{Ni}_2\text{O}_7$ under pressure, [Phys. Rev. Lett. **131**, 126001 \(2023\)](#).
- [48] Q.-G. Yang, D. Wang, and Q.-H. Wang, Possible S_{\pm} -wave superconductivity in $\text{La}_3\text{Ni}_2\text{O}_7$, [Phys. Rev. B **108**, L140505 \(2023\)](#).
- [49] Y.-B. Liu, J.-W. Mei, F. Ye, W.-Q. Chen, and F. Yang, s^{\pm} -wave pairing and the destructive role of apical-oxygen deficiencies in $\text{La}_3\text{Ni}_2\text{O}_7$ under pressure, [Phys. Rev. Lett. **131**, 236002 \(2023\)](#).
- [50] F. Lechermann, J. Gondolf, S. Bötzel, and I. M. Eremin, Electronic correlations and superconducting instability

- in $\text{La}_3\text{Ni}_2\text{O}_7$ under high pressure, *Phys. Rev. B* **108**, L201121 (2023).
- [51] H. Sakakibara, N. Kitamine, M. Ochi, and K. Kuroki, Possible high T_c superconductivity in $\text{La}_3\text{Ni}_2\text{O}_7$ under high pressure through manifestation of a nearly half-filled bilayer Hubbard model, *Phys. Rev. Lett.* **132**, 106002 (2024).
- [52] Y. Gu, C. Le, Z. Yang, X. Wu, and J. Hu, Effective model and pairing tendency in bilayer Ni-based superconductor $\text{La}_3\text{Ni}_2\text{O}_7$, [arXiv:2306.07275](https://arxiv.org/abs/2306.07275) (2023).
- [53] Y. Zhang, L.-F. Lin, A. Moreo, T. A. Maier, and E. Dagotto, Structural phase transition, s_{\pm} -wave pairing, and magnetic stripe order in bilayered superconductor $\text{La}_3\text{Ni}_2\text{O}_7$ under pressure, *Nat. Commun.* **15**, 2470 (2024).
- [54] C. Lu, Z. Pan, F. Yang, and C. Wu, Interlayer-coupling-driven high-temperature superconductivity in $\text{La}_3\text{Ni}_2\text{O}_7$ under pressure, *Phys. Rev. Lett.* **132**, 146002 (2024).
- [55] H. Oh and Y.-H. Zhang, Type-II t - J model and shared superexchange coupling from Hund's rule in superconducting $\text{La}_3\text{Ni}_2\text{O}_7$, *Phys. Rev. B* **108**, 174511 (2023).
- [56] Z. Liao, L. Chen, G. Duan, Y. Wang, C. Liu, R. Yu, and Q. Si, Electron correlations and superconductivity in $\text{La}_3\text{Ni}_2\text{O}_7$ under pressure tuning, *Phys. Rev. B* **108**, 214522 (2023).
- [57] X.-Z. Qu, D.-W. Qu, J. Chen, C. Wu, F. Yang, W. Li, and G. Su, Bilayer t - J - J_{\perp} model and magnetically mediated pairing in the pressurized nickelate $\text{La}_3\text{Ni}_2\text{O}_7$, *Phys. Rev. Lett.* **132**, 036502 (2024).
- [58] Y.-f. Yang, G.-M. Zhang, and F.-C. Zhang, Interlayer valence bonds and two-component theory for high- T_c superconductivity of $\text{La}_3\text{Ni}_2\text{O}_7$ under pressure, *Phys. Rev. B* **108**, L201108 (2023).
- [59] K. Jiang, Z. Wang, and F.-C. Zhang, High temperature superconductivity in $\text{La}_3\text{Ni}_2\text{O}_7$, *Chin. Phys. Lett.* (2023).
- [60] Y. Zhang, L.-F. Lin, A. Moreo, T. A. Maier, and E. Dagotto, Trends in electronic structures and s_{\pm} -wave pairing for the rare-earth series in bilayer nickelate superconductor $R_3\text{Ni}_2\text{O}_7$, *Phys. Rev. B* **108**, 165141 (2023).
- [61] Q. Qin and Y.-f. Yang, High- t_c superconductivity by mobilizing local spin singlets and possible route to higher t_c in pressurized $\text{La}_3\text{Ni}_2\text{O}_7$, *Phys. Rev. B* **108**, L140504 (2023).
- [62] Y.-H. Tian, Y. Chen, J.-M. Wang, R.-Q. He, and Z.-Y. Lu, Correlation effects and concomitant two-orbital s_{\pm} -wave superconductivity in $\text{La}_3\text{Ni}_2\text{O}_7$ under high pressure, *Phys. Rev. B* **109**, 165154 (2024).
- [63] R. Jiang, J. Hou, Z. Fan, Z.-J. Lang, and W. Ku, Pressure driven fractionalization of ionic spins results in cupratelike high- T_c superconductivity in $\text{La}_3\text{Ni}_2\text{O}_7$, *Phys. Rev. Lett.* **132**, 126503 (2024).
- [64] D.-C. Lu, M. Li, Z.-Y. Zeng, W. Hou, J. Wang, F. Yang, and Y.-Z. You, Superconductivity from doping symmetric mass generation insulators: Application to $\text{La}_3\text{Ni}_2\text{O}_7$ under pressure, [arXiv:2308.11195](https://arxiv.org/abs/2308.11195) (2023).
- [65] N. Kitamine, M. Ochi, and K. Kuroki, Theoretical designing of multiband nickelate and palladate superconductors with $d^{8+\delta}$ configuration, [arXiv:2308.12750](https://arxiv.org/abs/2308.12750) (2023).
- [66] Z. Luo, B. Lv, M. Wang, W. Wú, and D.-X. Yao, High- T_c superconductivity in $\text{La}_3\text{Ni}_2\text{O}_7$ based on the bilayer two-orbital t - J model, *npj Quantum Mater.* **9**, 61 (2024).
- [67] J.-X. Zhang, H.-K. Zhang, Y.-Z. You, and Z.-Y. Weng, Strong pairing originated from an emergent \mathbb{Z}_2 berry phase in $\text{La}_3\text{Ni}_2\text{O}_7$, *Phys. Rev. Lett.* **133**, 126501 (2024).
- [68] Z. Pan, C. Lu, F. Yang, and C. Wu, Effect of rare-earth element substitution in superconducting $\text{r}_3\text{ni}_2\text{o}_7$ under pressure, *Chin. Phys. Lett.* **41**, 087401 (2024).
- [69] H. Lange, L. Homeier, E. Demler, U. Schollwöck, A. Bohrdt, and F. Grusdt, Pairing dome from an emergent feshbach resonance in a strongly repulsive bilayer model, *Phys. Rev. B* **110**, L081113 (2024).
- [70] H. Yang, H. Oh, and Y.-H. Zhang, Strong pairing from doping-induced feshbach resonance and second fermi liquid through doping a bilayer spin-one mott insulator: application to $\text{La}_3\text{Ni}_2\text{O}_7$, [arXiv:2309.15095](https://arxiv.org/abs/2309.15095) (2023).
- [71] H. Lange, L. Homeier, E. Demler, U. Schollwöck, F. Grusdt, and A. Bohrdt, Feshbach resonance in a strongly repulsive ladder of mixed dimensionality: A possible scenario for bilayer nickelate superconductors, *Phys. Rev. B* **109**, 045127 (2024).
- [72] T. Kaneko, H. Sakakibara, M. Ochi, and K. Kuroki, Pair correlations in the two-orbital hubbard ladder: Implications for superconductivity in the bilayer nickelate $\text{La}_3\text{Ni}_2\text{O}_7$, *Phys. Rev. B* **109**, 045154 (2024).
- [73] X.-Z. Qu, D.-W. Qu, W. Li, and G. Su, Roles of Hund's rule and hybridization in the two-orbital model for high- t_c superconductivity in the bilayer nickelate, [arXiv:2311.12769](https://arxiv.org/abs/2311.12769) (2023).
- [74] M. Kakoi, T. Kaneko, H. Sakakibara, M. Ochi, and K. Kuroki, Pair correlations of the hybridized orbitals in a ladder model for the bilayer nickelate $\text{La}_3\text{Ni}_2\text{O}_7$, *Phys. Rev. B* **109**, L201124 (2024).
- [75] Z. Fan, J.-F. Zhang, B. Zhan, D. Lv, X.-Y. Jiang, B. Normand, and T. Xiang, Superconductivity in nickelate and cuprate superconductors with strong bilayer coupling, *Phys. Rev. B* **110**, 024514 (2024).
- [76] X. Wu, H. Yang, and Y.-H. Zhang, Deconfined fermi liquid to fermi liquid transition and superconducting instability, *Phys. Rev. B* **110**, 125122 (2024).
- [77] Y. Zhang, L.-F. Lin, A. Moreo, T. A. Maier, and E. Dagotto, Electronic structure, self-doping, and superconducting instability in the alternating single-layer trilayer stacking nickelates $\text{La}_3\text{Ni}_2\text{O}_7$, *Phys. Rev. B* **110**, L060510 (2024).
- [78] S. Ryeong, N. Witt, and T. O. Wehling, Quenched pair breaking by interlayer correlations as a key to superconductivity in $\text{La}_3\text{Ni}_2\text{O}_7$, *Phys. Rev. Lett.* **133**, 096002 (2024).
- [79] X.-S. Ni, Y. Ji, L. He, T. Xie, D.-X. Yao, M. Wang, and K. Cao, Spin density wave in the bilayered nickelate $\text{La}_3\text{Ni}_2\text{O}_{7-\delta}$ at ambient pressure, [arXiv:2407.19213](https://arxiv.org/abs/2407.19213) (2024).
- [80] C. Lu, Z. Pan, F. Yang, and C. Wu, Interplay of two E_g orbitals in superconducting $\text{La}_3\text{Ni}_2\text{O}_7$ under pressure, *Phys. Rev. B* **110**, 094509 (2024).
- [81] Z. Ouyang, M. Gao, and Z.-Y. Lu, Absence of electron-phonon coupling superconductivity in the bilayer phase of $\text{La}_3\text{Ni}_2\text{O}_7$ under pressure, *npj Quantum Materials* **9**, 80 (2024).
- [82] Y.-B. Liu, H. Sun, M. Zhang, Q. Liu, W.-Q. Chen, and F. Yang, Origin of the diagonal double-stripe spin-density-wave and potential superconductivity in bulk $\text{La}_3\text{Ni}_2\text{O}_7$ at ambient pressure, [arXiv:2501.14752](https://arxiv.org/abs/2501.14752)

- (2024).
- [83] C. Yue, J.-J. Miao, H. Huang, Y. Hua, P. Li, Y. Li, G. Zhou, W. Lv, Q. Yang, H. Sun, *et al.*, Correlated electronic structures and unconventional superconductivity in bilayer nickelate heterostructures, [arXiv:2501.06875 \(2025\)](#).
- [84] Y. Wang, Z. Chen, Y. Zhang, K. Jiang, and J. Hu, The mottness and the anderson localization in bilayer nickelate $\text{La}_3\text{Ni}_2\text{O}_7$, [arXiv:2501.08536 \(2025\)](#).
- [85] E. K. Ko, Y. Yu, Y. Liu, L. Bhatt, J. Li, V. Thampy, C.-T. Kuo, B. Y. Wang, Y. Lee, K. Lee, *et al.*, Signatures of ambient pressure superconductivity in thin film $\text{La}_3\text{Ni}_2\text{O}_7$, *Nature*, **1** (2024).
- [86] G. Zhou, W. Lv, H. Wang, Z. Nie, Y. Chen, Y. Li, H. Huang, W. Chen, Y. Sun, Q.-K. Xue, and Z. Chen, Ambient-pressure superconductivity onset above 40 k in bilayer nickelate ultrathin films, [arXiv:2412.16622 \(2024\)](#).
- [87] P. Li, G. Zhou, W. Lv, Y. Li, C. Yue, H. Huang, L. Xu, J. Shen, Y. Miao, W. Song, *et al.*, Photoemission evidence for multi-orbital hole-doping in superconducting $\text{La}_{2.85}\text{Pr}_{0.15}\text{Ni}_2\text{O}_7/\text{SrLaAlO}_4$ interfaces, [arXiv:2501.09255 \(2025\)](#).
- [88] L. Bhatt, A. Y. Jiang, E. K. Ko, N. Schnitzer, G. A. Pan, D. F. Segedin, Y. Liu, Y. Yu, Y.-F. Zhao, E. A. Morales, *et al.*, Resolving structural origins for superconductivity in strain-engineered $\text{La}_3\text{Ni}_2\text{O}_7$ thin films, [arXiv:2501.08204 \(2025\)](#).
- [89] Y. Liu, E. K. Ko, Y. Tarn, L. Bhatt, B. H. Goodge, D. A. Muller, S. Raghu, Y. Yu, and H. Y. Hwang, Superconductivity and normal-state transport in compressively strained $\text{La}_2\text{PrNi}_2\text{O}_7$ thin films, [arXiv:2501.08022 \(2025\)](#).
- [90] H. Zhong, Y. Wei, Z. Zhang, R. Liu, X. Huang, X.-S. Ni, M. d. R. Cantarino, K. Cao, Y. Nie, T. Schmitt, *et al.*, Epitaxial strain tuning of electronic and spin excitations in $\text{La}_3\text{Ni}_2\text{O}_7$ thin films, [arXiv:2502.03178 \(2025\)](#).
- [91] Q. Li, Y.-J. Zhang, Z.-N. Xiang, Y. Zhang, X. Zhu, and H.-H. Wen, Signature of superconductivity in pressurized $\text{La}_4\text{Ni}_3\text{O}_{10}$, *Chin. Phys. Lett.* **41**, 017401 (2024).
- [92] Y. Zhu, D. Peng, E. Zhang, B. Pan, X. Chen, L. Chen, H. Ren, F. Liu, Y. Hao, N. Li, *et al.*, Superconductivity in pressurized trilayer $\text{La}_4\text{Ni}_3\text{O}_{10-\delta}$ single crystals, *Nature* **631**, 531 (2024).
- [93] M. Zhang, C. Pei, X. Du, Y. Cao, Q. Wang, J. Wu, Y. Li, Y. Zhao, C. Li, W. Cao, S. Zhu, Q. Zhang, N. Yu, P. Cheng, J. Zhao, Y. Chen, H. Guo, L. Yang, and Y. Qi, Superconductivity in trilayer nickelate $\text{La}_4\text{Ni}_3\text{O}_{10}$ under pressure, [arXiv:2311.07423 \(2023\)](#).
- [94] N. Yuan, A. Elghandour, J. Arneth, K. Dey, and R. Klingeler, High-pressure crystal growth and investigation of the metal-to-metal transition of ruddlesden–popper trilayer nickelates $\text{La}_4\text{Ni}_3\text{O}_{10}$, *J. Cryst. Growth* **627**, 127511 (2024).
- [95] H. Sakakibara, M. Ochi, H. Nagata, Y. Ueki, H. Sakurai, R. Matsumoto, K. Terashima, K. Hirose, H. Ohta, M. Kato, Y. Takano, and K. Kuroki, Theoretical analysis on the possibility of superconductivity in the trilayer ruddlesden–popper nickelate $\text{La}_4\text{Ni}_3\text{O}_{10}$ under pressure and its experimental examination: Comparison with $\text{La}_3\text{Ni}_2\text{O}_7$, *Phys. Rev. B* **109**, 144511 (2024).
- [96] J. Li, C.-Q. Chen, C. Huang, Y. Han, M. Huo, X. Huang, P. Ma, Z. Qiu, J. Chen, X. Hu, L. Chen, T. Xie, B. Shen, H. Sun, D. Yao, and M. Wang, Structural transition, electric transport, and electronic structures in the compressed trilayer nickelate $\text{La}_4\text{Ni}_3\text{O}_{10}$, *Sci. China- Phys. Mech. Astron.* **67**, 117403 (2024).
- [97] M. Kakoi, T. Oi, Y. Ohshita, M. Yashima, K. Kuroki, T. Kato, H. Takahashi, S. Ishiwata, Y. Adachi, N. Hatada, T. Uda, and H. Mukuda, Multiband metallic ground state in multilayered nickelates $\text{La}_3\text{Ni}_2\text{O}_7$ and $\text{La}_4\text{Ni}_3\text{O}_{10}$ probed by ^{139}La -nmr at ambient pressure, *J. Phys. Soc. Jpn.* **93**, 053702 (2024).
- [98] I. V. Leonov, Electronic structure and magnetic correlations in the trilayer nickelate superconductor $\text{La}_4\text{Ni}_3\text{O}_{10}$ under pressure, *Phys. Rev. B* **109**, 235123 (2024).
- [99] P.-F. Tian, H.-T. Ma, X. Ming, X.-J. Zheng, and H. Li, Effective model and electron correlations in trilayer nickelate superconductor $\text{La}_4\text{Ni}_3\text{O}_{10}$, *J. Condens. Matter Phys.* **36**, 355602 (2024).
- [100] J.-X. Wang, Z. Ouyang, R.-Q. He, and Z.-Y. Lu, Non-fermi liquid and hund correlation in $\text{La}_4\text{Ni}_3\text{O}_{10}$ under high pressure, *Phys. Rev. B* **109**, 165140 (2024).
- [101] H. LaBollita, J. Kapeghian, M. R. Norman, and A. S. Botana, Electronic structure and magnetic tendencies of trilayer $\text{La}_4\text{Ni}_3\text{O}_{10}$ under pressure: Structural transition, molecular orbitals, and layer differentiation, *Phys. Rev. B* **109**, 195151 (2024).
- [102] Y. Zhang, L.-F. Lin, A. Moreo, T. A. Maier, and E. Dagotto, Prediction of s^\pm -wave superconductivity enhanced by electronic doping in trilayer nickelates $\text{La}_4\text{Ni}_3\text{O}_{10}$ under pressure, *Phys. Rev. Lett.* **133**, 136001 (2024).
- [103] Q.-G. Yang, K.-Y. Jiang, D. Wang, H.-Y. Lu, and Q.-H. Wang, Effective model and s^\pm -wave superconductivity in trilayer nickelate $\text{La}_4\text{Ni}_3\text{O}_{10}$, *Phys. Rev. B* **109**, L220506 (2024).
- [104] C.-Q. Chen, Z. Luo, M. Wang, W. Wú, and D.-X. Yao, Trilayer multiorbital models of $\text{La}_4\text{Ni}_3\text{O}_{10}$, *Phys. Rev. B* **110**, 014503 (2024).
- [105] M. Zhang, H. Sun, Y.-B. Liu, Q. Liu, W.-Q. Chen, and F. Yang, The s^\pm -wave superconductivity in the pressurized $\text{La}_4\text{Ni}_3\text{O}_{10}$, *Phys. Rev. B* **110**, L180501 (2024).
- [106] F. Lechermann, S. Bötzel, and I. M. Eremin, Electronic instability, layer selectivity, and fermi arcs in $\text{La}_3\text{Ni}_2\text{O}_7$, *Phys. Rev. Mater.* **8**, 074802 (2024).
- [107] J. Huang and T. Zhou, Interlayer pairing-induced partially gapped fermi surface in trilayer $\text{La}_4\text{Ni}_3\text{O}_{10}$ superconductors, *Phys. Rev. B* **110**, L060506 (2024).
- [108] H. Oh, B. Zhou, and Y.-H. Zhang, Type-ii t-j model in charge transfer regime in bilayer $\text{La}_3\text{Ni}_2\text{O}_7$ and trilayer $\text{La}_4\text{Ni}_3\text{O}_{10}$, *Phys. Rev. B* **111**, L020504 (2025).
- [109] Q. Qin, J. Wang, and Y. feng Yang, Frustrated superconductivity and intrinsic reduction of t_c in trilayer nickelate, *The Innovation Materials* **2**, 100102 (2024).
- [110] S. Xu, C.-Q. Chen, M. Huo, D. Hu, H. Wang, Q. Wu, R. Li, D. Wu, M. Wang, D.-X. Yao, *et al.*, Origin of the density wave instability in trilayer nickelate $\text{La}_4\text{Ni}_3\text{O}_{10}$ revealed by optical and ultrafast spectroscopy, [arXiv:2405.19161 \(2024\)](#).
- [111] X. Du, Y. Li, Y. Cao, C. Pei, M. Zhang, W. Zhao, K. Zhai, R. Xu, Z. Liu, Z. Li, *et al.*, Correlated electronic structure and density-wave gap in trilayer nickelate $\text{La}_4\text{Ni}_3\text{O}_{10}$, [arXiv:2405.19853 \(2024\)](#).
- [112] Z. Huo, P. Zhang, Z. Zhang, D. Duan, and T. Cui, Electronic correlations and hund’s rule coupling in trilayer nickelate $\text{La}_4\text{Ni}_3\text{O}_{10}$, [arXiv:2407.00327 \(2024\)](#).
- [113] Y.-f. Yang, Decomposition of multilayer superconduc-

- tivity with interlayer pairing, *Phys. Rev. B* **110**, 104507 (2024).
- [114] Y. Zhang, L.-F. Lin, A. Moreo, T. A. Maier, and E. Dagotto, Magnetic correlations and pairing tendencies of the hybrid stacking nickelate superlattice $\text{La}_7\text{Ni}_5\text{O}_{17}$ ($\text{La}_3\text{Ni}_2\text{O}_7/\text{La}_4\text{Ni}_3\text{O}_{10}$) under pressure, [arXiv:2408.07690](https://arxiv.org/abs/2408.07690) (2024).
- [115] X. Huang, H. Zhang, J. Li, M. Huo, J. Chen, Z. Qiu, P. Ma, C. Huang, H. Sun, and M. Wang, Signature of superconductivity in pressurized trilayer-nickelate $\text{Pr}_4\text{Ni}_3\text{O}_{10-\delta}$, *Chin. Phys. Lett.* **41**, 127403 (2024).
- [116] Z. Liu, J. Li, M. Huo, B. Ji, J. Hao, Y. Dai, M. Ou, Q. Li, H. Sun, B. Xu, Y. Lu, M. Wang, and H.-H. Wen, Evolution of electronic correlations in the ruddlesden-popper nickelates, [arXiv:2411.08539](https://arxiv.org/abs/2411.08539) (2024).
- [117] S. Deswal, D. Kumar, D. Rout, S. Singh, and P. Kumar, Dynamics of electron-electron correlated to electron-phonon coupled phase progression in trilayer nickelate $\text{La}_4\text{Ni}_3\text{O}_{10}$, [arXiv:2411.13933](https://arxiv.org/abs/2411.13933) (2024).
- [118] Y.-F. Zhao and A. S. Botana, Electronic structure of ruddlesden-popper nickelates: strain to mimic the effects pressure, [arXiv:2412.04391](https://arxiv.org/abs/2412.04391) (2024).
- [119] M. Shi, D. Peng, K. Fan, Z. Xing, S. Yang, Y. Wang, H. Li, R. Wu, M. Du, B. Ge, *et al.*, Superconductivity of the hybrid ruddlesden-popper $\text{La}_5\text{Ni}_3\text{O}_{11}$ single crystals under high pressure, [arXiv:2502.01018](https://arxiv.org/abs/2502.01018) (2025).
- [120] J. Li, P. Ma, H. Zhang, X. Huang, C. Huang, M. Huo, D. Hu, Z. Dong, C. He, J. Liao, X. Chen, T. Xie, H. Sun, and M. Wang, Pressure-driven right-triangle shape superconductivity in bilayer nickelate $\text{La}_3\text{Ni}_2\text{O}_7$, [arXiv:2404.11369](https://arxiv.org/abs/2404.11369) (2024).
- [121] Y. Zhang, L.-F. Lin, A. Moreo, T. A. Maier, and E. Dagotto, Electronic structure, magnetic correlations, and superconducting pairing in the reduced ruddlesden-popper bilayer $\text{La}_3\text{Ni}_2\text{O}_6$ under pressure: Different role of $d_{3z^2-r^2}$ orbital compared with $\text{La}_3\text{Ni}_2\text{O}_7$, *Phys. Rev. B* **109**, 045151 (2024).
- [122] G. Kotliar and J. Liu, Superexchange mechanism and d-wave superconductivity, *Phys. Rev. B* **38**, 5142 (1988).
- [123] P. A. Lee, N. Nagaosa, and X.-G. Wen, Doping a mott insulator: Physics of high-temperature superconductivity, *Rev. Mod. Phys.* **78**, 17 (2006).

Acknowledgments

We are grateful to the discussions with Yu-Bo Liu and Hongyi Sun. This work is supported by the NSFC under Grant Nos.12234016, 12074031, 12141402, 12334002 and 12304180. Ming Zhang is supported by Zhejiang Provincial Natural Science Foundation of China under Grant No. ZCLQN25A0402.

Author contribution

Fan Yang designed the project. Chen Lu and Ming Zhang carried out numerical calculations for SBMF calculations. Ming Zhang, Chen Lu, Zhiming Pan and Fan Yang wrote the manuscript. All co-authors provided useful comments and discussion on the paper.

Competing interests

The authors declare no competing interests.

Addition information

Supplementary information The online version contains supplementary information available at